Journal of Molecular Graphics and Modelling 49 (2014) 110–117

Contents lists available at ScienceDirect

Journal of Molecular Graphics and Modelling

journal homepage: www.elsevier.com/locate/JMGM

Design of an interface peptide as new inhibitor of human glucose-6-phosphate dehydrogenase

Cristian Obiol-Pardo[a,1], Gema Alcarraz-Vizán[b,1,2], Santiago Díaz-Moralli[b], Marta Cascante[b,*], Jaime Rubio-Martinez[a,*]

[a] Departament de Química Física, University of Barcelona and Institut de Recerca en Química Teòrica i Computacional (XRQTC). Martí i Franquès 1, 08028 Barcelona, Spain
[b] Departament de Bioquímica i Biologia Molecular, Facultat de Biologia, Institut de Biomedicina, University of Barcelona (IBUB) and IDIBAPS-Hospital Clinic, Barcelona, Spain

ARTICLE INFO

Article history:
Received 10 January 2014
Received in revised form 18 February 2014
Accepted 19 February 2014
Available online 28 February 2014

Keywords:
Glucose-6-phosphate dehydrogenase
Interface peptides
Molecular modeling
MMPBSA
Cancer

ABSTRACT

Glucose-6-phosphate dehydrogenase (G6PDH) is an essential enzyme involved in the first reaction of the oxidative branch of the pentose phosphate pathway (PPP). Recently, G6PDH was suggested as a novel target protein for cancer therapy as one of the final products of the PPP, ribose-5-phosphate, is necessary for nucleic acid synthesis and tumor progression. After analyzing the protein–protein interface of the crystal structure of human G6PDH by means of molecular dynamics simulations, we designed six interface peptides based on the natural sequence of the protein. The three most promising peptides, as predicted by binding free energy calculations, were synthesized and one of them was confirmed as a novel inhibitor of human G6PDH in experimental assays. Together, the active peptide found and its suggested binding mode proposes a new strategy for inhibiting this enzyme and should aid the further design of novel, potent and non-peptidic G6PDH inhibitors.

1. Introduction

Human glucose-6-phosphate dehydrogenase (G6PDH, EC 1.1.1.49) is a $NADP^+$-dependent homodimeric enzyme that catalyzes the transformation of D-glucose-6-phosphate into 6-phosphogluconolactone in the first step of the oxidative branch of the pentose phosphate pathway (PPP) [1]. This pathway generates NADPH molecules that protect the cell against oxidative stress. PPP also generates ribose-5-phosphate, an essential metabolite for nucleic acid synthesis. G6PDH has been reported as the enzyme with highest control coefficient over the flux of the oxidative branch of the PPP [2] and furthermore, several recent studies showed that G6PDH can be considered as a novel target for anti-cancer chemotherapy due to its essential role in maintaining the reduced antioxidant pool and in protecting the cell from oxidative stress [3–5]. Thus, throughout this branch ribose is synthesized and the reducing power necessary for fatty acid synthesis and for cell protection against oxidative damage is obtained [6,7]. Despite the importance of this enzyme no efficient inhibitors have been found up to date. Methotrexate [8] and dehydroepiandrosterone (DHEA) [9] are well known inhibitors of G6PDH, but the former is not specific and inhibits other $NADP^+$-dependent enzymes whereas DHEA, due to its hormone structure, affects many other cellular mechanisms and pathways. A novel class of compounds, represented by KPF-CoA, was recently discovered as G6PDH dimer disruptors [10], but they exhibited only modest activity. Additionally, combination of drugs such as cefaperazone/sulbactam [11] or ampicillin/sulbactam [11] inhibits G6PDH in a competitive and non-competitive manner, respectively, but little information is available about the binding site or mechanism of action of these compounds. Metamizol was also found to interfere with G6PDH activity [12].

As the crystal structure of human G6PDH is available [13], we carried out a molecular dynamics simulation to analyze the strongest contact points of the G6PDH homodimer, and further designed six interface peptides, including a cyclic peptide, as potential new inhibitors of the protein by disruption of the monomer–monomer interactions. The approach of targeting homodimeric enzymes has been recently reviewed [14].

* Corresponding authors.
E-mail addresses: martacascante@ub.edu (M. Cascante), jaime.rubio@ub.edu (J. Rubio-Martinez).
[1] These authors contributed equally to this study.
[2] Current address: Diabetes and Obesity Laboratory, Institut d'Investigacions Biomèdiques August Pi i Sunyer (IDIBAPS), Centre Esther Koplowitz (CEK), Rosselló 149-153, 08036 Barcelona, Spain.

http://dx.doi.org/10.1016/j.jmgm.2014.02.004
1093-3263/

It is known that the $NADP^+$ cofactors stabilize the G6PDH homodimer structure and point mutations at the protein-protein interface affect the $NADP^+$ binding site and the enzyme catalytical activity [13,15]. It is therefore possible to inhibit G6PDH by distorting its dimer interface.

Peptides are ideal starting candidates to design inhibitors as they are able to interact within the extended, non-consecutive and flat surface of protein–protein interfaces [16]. Some examples of interface peptide inhibitors can be found elsewhere [17,18]. Recently, novel peptides with cytotoxic activity were designed by using information coming from molecular modeling [19]. Moreover, targeting protein–protein interactions to modify the interactome of the cell is changing the paradigm in drug discovery [20].

Although not presenting proper drug-like properties, peptides can be useful to further design small peptidomimetic molecules by retaining part of the interactions found in the peptide–protein system.

After predicting the affinity of six designed peptides by binding free energy calculations, three promising candidates were synthesized and one peptide of 14 residues was confirmed to be active in experimental assays. This peptide provides novel insights into the inhibition of human G6PDH.

2. Methods

All calculations described in the present study were carried out at the molecular mechanics level, using the amber force field [21] as implemented in the Amber 10 suite of programs [22]. The solvent was considered explicitly and the cut-off distance was kept to 9 Å to compute the non-bonded non-polar interactions. All simulations were carried out under periodic boundary conditions. Long-range electrostatic interactions were treated by means of the particle-mesh Ewald method [23] as implemented in Amber. All structural figures of the present study were prepared with the VMD software [24].

2.1. Preparation of the human G6PDH homodimer

The initial 3D structure of human G6PDH was downloaded from the Protein Data Bank, with entry code 1QKI [13]. As the minimum functional complex, we selected chains A and B for obtaining the G6PDH homodimer, due to the tetrameric structure of the enzyme is pH dependent presenting a rapid tetramer-dimer equilibrium [13]. The crystallized structure represents the G6PDH with the Canton mutation; this mutation was changed backwards in order to obtain the wild-type protein by using the Leap program of Amber. Glycerol and glycolic acid molecules were removed from the structure, whereas structural waters were maintained. Residues 1 to 26 of chain A and 1 to 27 of chain B were removed for presenting crystallographic data with low resolution. These residues are at an approximate distance of 30 Å from the dimer interface and thus we can assume that they have no influence in our simulations.

Leap program of the Amber suite was used to add hydrogen atoms, to neutralize the system with an appropriate number of sodium counterions, to solvate the system with a complete cubic box of TIP3P water model and to update the force field parameters of the $NADP^+$ cofactors, which were adapted from the Ryde set [25]. The final system consisted in G6PDH subunits A and B, two $NADP^+$ as cofactor molecules, eleven sodium counterions and a cubic box of 43,000 water molecules. Dimensions of the water box were $x = 107$ Å, $y = 126$ Å and $z = 105$ Å.

2.2. Molecular dynamics simulation

The G6PDH homodimer was energy-minimized in order to remove steric stress by means of a multi-step procedure. First, only water and counterion molecules were minimized constraining the remaining part of the system. Second, side chains of the protein were also minimized while protein backbone and cofactors remained constrained. Third, $NADP^+$ molecules were minimized as well as the protein backbone and finally all atoms were minimized by using 100,000 iterations combining the steepest descent and the conjugated gradient algorithms until a final energy gradient of 1.1 kcal/mol.

The minimized structure was subjected to a molecular dynamics simulation. It started by heating up the system to 300 K, coupling the system to a thermal bath with the Berendsen's algorithm [26] and a time coupling constant of 0.2 ps and incrementing the temperature using a constant rate of 30 K/10 ps. Once the density of the system was equilibrated by applying a pressure-constant step of 40 ps, molecular dynamics was carried out using the SHAKE algorithm [27] within the NVT ensemble along 2.5 ns of production run. Last nanosecond of converged total energy was used as production time for analyzing the stability of the protein–protein contacts.

2.3. Preparation and molecular dynamics of the peptide-G6PDH systems

Based on the equilibrated structure of the G6PDH homodimer, the starting structures of six peptide-G6PDH systems were prepared by retaining one subunit of the protein and utilizing the corresponding part of the second one for modeling each peptide. The $NADP^+$ molecule belonging to the entire monomer was retained. The cyclic peptide was derived from the natural sequence of the protein by adding two new glycine residues and creating the amide bond by means of the Leap program of Amber. After preparing all systems with the Leap program as described before for the G6PDH homodimer, they were submitted to equivalent minimizations (employing 50,000 iterations until energy gradients below 2 kcal/mol) and molecular dynamics simulations (2.5 ns of production run). Last nanosecond of converged total energy was used as production time for analyzing the stability of the peptide–protein contacts.

2.4. Binding free energy calculation of the peptide-G6PDH systems

The MMPB(GB)SA protocol [28] was used to predict the binding free energy of each peptide to G6PDH by extracting one hundred equidistant snapshots of each molecular dynamics simulation.

This method was used within the one-trajectory protocol that avoids calculating three separate molecular dynamics runs (for complex, ligand and receptor) and improves internal consistency. Molecular mechanics (MM) energies, representing internal, electrostatic and van der Waals components were extracted from the amber force field. Electrostatic solvation contribution to binding was calculated by means of the Poisson-Boltzmann (PB) or Generalized Born (GB) equations. For the latter, the parametrization of Tsui and Case [29] was utilized. Parse radii set was used both in PB and GB contributions. External and internal dielectric constants of 80.0 and 1.0, respectively, were used for the calculation. Non polar solvation effect was computed by using a linear relationship with the solvent accessible surface area (SASA) with a slope of 0.00542 kcal/mol$Å^2$ and 0.0072 kcal/mol$Å^2$ for the PB and GB contributions, respectively, and an intercept of 0.92 kcal/mol and 0.00 kcal/mol for the PB and GB contributions, respectively. Finally, entropic effects were computed through a normal mode analysis with the nmode module of amber before a minimization routine up to an energy gradient lower than 10^{-4} kcal/mol. Due to the computational cost of the entropy calculation, ten structures were extracted from the production dynamics and the G6PDH monomer was cut to only those residues located within a cutoff

distance of 12 Å from the center of masses of each peptide. The $NADP^+$ molecule was included as part of the receptor when it belonged to the predefined cutoff.

3. Experimental

3.1. Peptide synthesis

Peptides were synthesized in an Abi433A synthesizer (Applied Biosystems) using FasMoc protocol. Couplings were carried out in an Fmoc-Gly-2-chlorotrityl resin using TBTU/HOBt as a coupling agent. Linear peptides were eluted from the resin with TFA 1% in DCM and the cyclic peptide was cycled with PyBOP/HOAt in DCM/DMF (9:1). Side chains were deprotected using TFA/water/triethylsylane (95:2.5:2.5). Then, peptides were purified by preparative high pressure liquid chromatography (HPLC) in a Waters DeltaPrep 4000 (Waters Symmetry C18 column) in MeCN gradient (5–20%). The final products were characterized by matrix assisted laser desorption/ionization time-of-flight (MALDI-TOF) mass spectrometry in 4700 Proteomics Analyzer (Applied Biosystems) and by amino acid analysis through the HPLC AccQ.Tag (Waters) in a Delta 600 (Waters).

3.2. Human glucose-6-phosphate dehydrogenase purification

The construct based on the plasmid pKK233-2 containing full-length human cDNA coding for normal G6PDH has been previously described [30,31]. Wild-type G6PDH was purified to homogeneity by affinity chromatography on 2′,5′-ADP Sepharose 4B as described elsewhere [30,31]. The purity of the enzyme preparation was confirmed by SDS-PAGE.

3.3. Determination of glucose-6-phosphate dehydrogenase activity

Glucose-6-phosphate dehydrogenase activity was measured as described previously [32]. Briefly, pure G6PDH (purified as described above) was added to a cuvette containing 0.5 mM $NADP^+$ (Sigma-Aldrich Co, St. Louis, MO, USA) and 50 mM Tris–HCl, pH 7.6 at 37 °C. Reactions were initiated by the addition of glucose-6-phosphate (Sigma–Aldrich Co) to a final concentration of 2 mM. The reduction of $NADP^+$, which is directly proportional to G6PDH activity, was followed by the increase in absorbance at 340 nm.

4. Results

4.1. Analysis of the protein-protein interface of human G6PDH

The last nanosecond of molecular dynamics simulation (see Section 2) was utilized to analyze the stability of the protein–protein interface of G6PDH in order to find for the most stable contacts, suitable to be mimicked by a small compound. Accordingly with the crystal structure of the enzyme [13], the dimer interface is mainly formed by the mutual interaction of the so-called alpha and beta domains (Fig. 1) involving 57 residues within an area of 2856 $Å^2$. The alpha domain is composed by two perpendicular alpha helices belonging to the sequence E206-I230, of both monomers. The beta domain, on its own, is composed by two antiparallel beta sheets joined by a beta turn, belonging to the sequence D388-Y428, of both monomers. Firstly, the production time was used to identify the inter-subunit hydrogen bonds as shown in Table 1. The alpha domain maintained 8 stable hydrogen bonds with the partner monomer. Similarly, Table 2 shows the 20 inter-subunit hydrogen bonds formed in the beta domain. In corroboration with the crystal structure, the charged residues D421, E206, K407, E419 and R427 were involved in highly stable hydrogen bonds throughout the simulation. However our analysis also showed that N388 and N218, residues not highlighted in the crystal structure, maintained strong hydrogen bonds.

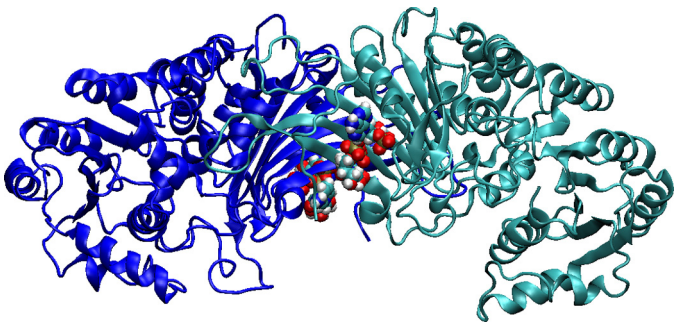

Fig. 1. Crystal structure of the homodimer of human G6PDH showing the $NADP^+$ cofactors.

Table 1
List of inter-subunit hydrogen bonds formed in the G6PDH alpha domain.

Hydrogen donor	Hydrogen acceptor	% Occupancy
N388 NH sc (B)	N218 O sc (A)	91.8
M405 NH mc (B)	N218 O sc (A)	98.5
K407 NH sc (B)	E206 O sc (A)	63.6
K407 NH mc (B)	N210 O sc (A)	97.2
G410 NH mc (B)	E206 O sc (A)	66.6
N210 NH sc (A)	T406 O sc (B)	69.8
N218 NH sc (A)	M405 O mc (B)	97.8
R219 NH_2 sc (A)	D375 O mc (B)	89.7

Per cent of occupancy defines the total simulation time that the geometry of the hydrogen bond is optimum: N-O distance < 3.3 Å and hydrogen bond angle between 180 ± 20°. G6PDH subunit marked in brackets, "sc" denotes for a side chain atom, whereas "mc" denotes for a main chain atom.

Table 2
List of inter-subunit hydrogen bonds formed in the G6PDH beta domain.

Hydrogen donor	Hydrogen acceptor	% Occupancy
N388 NH sc (A)	N218 O sc (B)	94.8
M405 NH mc (A)	N218 O sc (B)	96.8
T406 OH sc (A)	Y424 O sc (B)	92.7
K407 NH mc (A)	N210 O sc (B)	99.2
G410 NH mc (A)	E206 O sc (B)	91.0
S418 OH sc (A)	Y428 O sc (B)	78.6
D421 NH mc (A)	D421 O mc (B)	70.3
R427 NH_2 sc (A)	E419 O sc (B)	100
R427 NH_2 sc (A)	K508 O mc (B)	70.6
R427 NH sc (A)	E419 O sc (B)	98.5
N210 NH sc (B)	T406 O sc (A)	58.8
N218 NH sc (B)	M405 O mc (A)	96.5
R219 NH sc (B)	N388 O sc (A)	78.8
S418 OH sc (B)	Y428 O sc (A)	78.6
D421 NH mc (B)	D421 O mc (A)	98.8
Y424 OH sc (B)	K407 O mc (A)	96.5
R427 NH_2 sc (B)	E419 O sc (A)	100
R427 NH sc (B)	E419 O sc (A)	99.7
Y428 OH sc (B)	E416 O sc (A)	90.2
R439 NH_2 sc (B)	G410 O mc (A)	71.0

Per cent of occupancy defines the total simulation time that the geometry of the hydrogen bond is optimum: N-O distance < 3.3 Å and hydrogen bond angle between 180 ± 20°. G6PDH subunit marked in brackets, "sc" denotes for a side chain atom, whereas "mc" denotes for a main chain atom.

Figs. 2 and 3 show a deeper analysis of the dimer interface of G6PDH, pointing the average per residue of the intermolecular energies, both electrostatic and van der Waals components of the force field, extracted from the production dynamics. These results were utilized to identify the residues that participated most in stabilizing the dimer structure. High electrostatic energies were found in residues G206 and R219 of the alpha domain and in residues

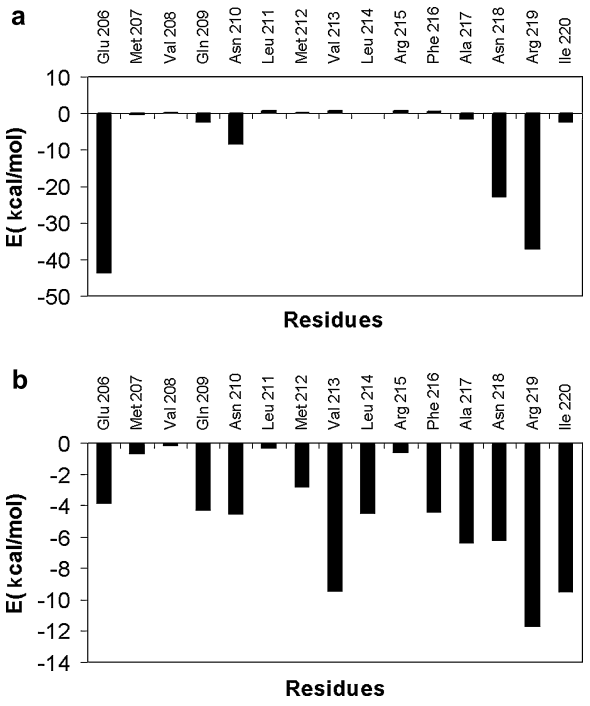

Fig. 2. Average electrostatic (a) and van der Waals (b) intermolecular energies of the main residues of G6PDH in the alpha domain.

K407, E419 and R427 of the beta domain. Similarly, R219, V213 and I220 maintained the strongest van der Waals contacts in the alpha domain, whereas a much more hydrophobic core formed by M404, F413, L420 and L422 was found in the beta domain. Particularly, those residues enclosed in the sequence K407-F413 that belongs to the beta turn of the beta domain, formed an intensive

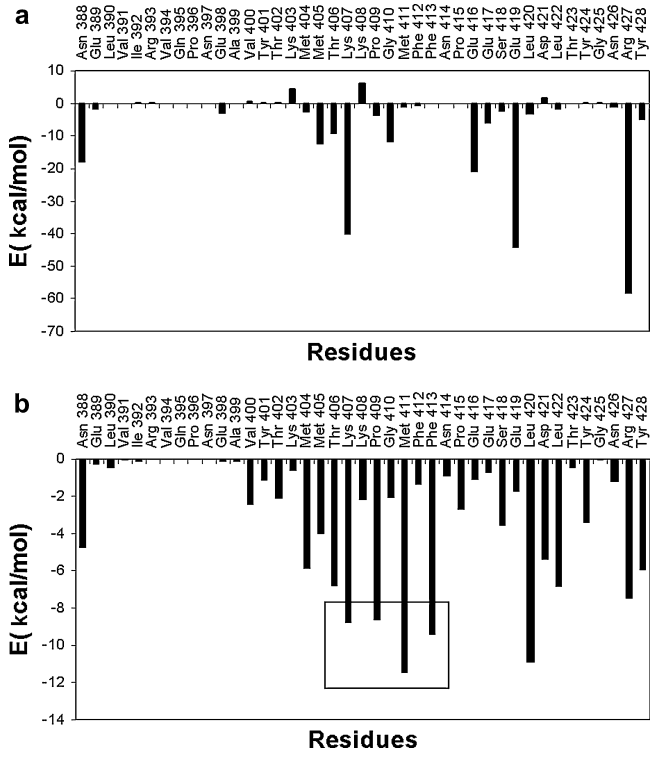

Fig. 3. Average electrostatic (a) and van der Waals (b) intermolecular energies of the main residues of G6PDH in the beta domain. A cluster of hydrophobic contacts is remarked in a box.

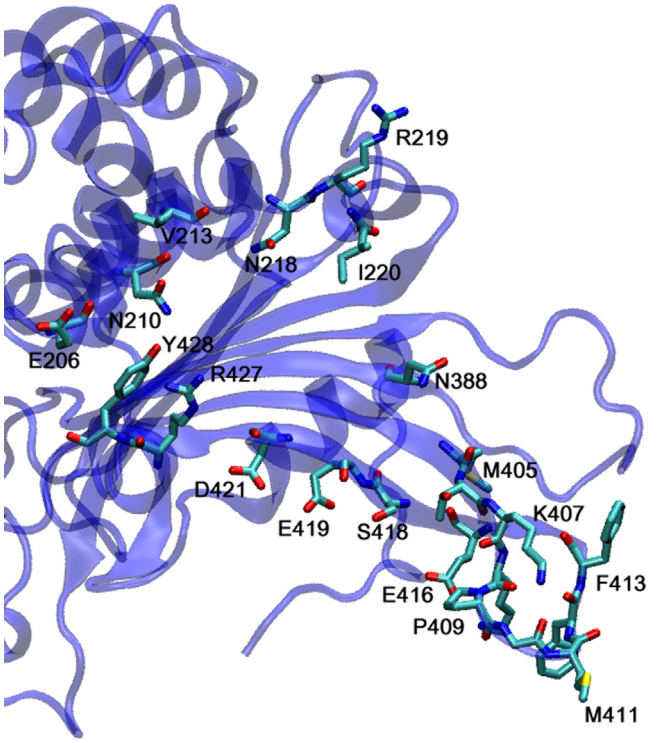

Fig. 4. Detailed view of residues of the first G6PDH subunit that established stable intermolecular interactions throughout molecular dynamics (hydrogen atoms not shown for simplicity).

interaction pattern with the partner monomer. Thus, this sequence maintained nine interaction points distributed in: a salt bridge in K407, four hydrogen bonds in K407 and G410 and four hydrophobic contacts in K407, P409, M411 and F413. Importance of G410 was highlighted in the mutants G410C and G410D, which lowered the thermostability of G6PDH [13]. The complexity of the dimer recognition is illustrated in Fig. 4, where the main residues that established either hydrogen bonds or van der Waals interactions in the first G6PDH subunit are specified.

4.2. Design of interface peptides and analysis of their binding affinities

The analysis of protein–protein contacts described in the above section was utilized to configure six interface peptides whose natural sequences belonged to the most important contacts (hot spots) of the homodimer of G6PDH (see Section 2). Moreover, proximity to the catalytical site containing $NADP^+$, and presence of secondary structure elements were also considered in designing the peptides. Sequences of these peptides are as follows:

Peptide 1: K^{205}-E-M-V-Q-N-L-M-V-L-R-F-A-N-R-I^{220}
Peptide 2: N^{218}-R-I-F-G-P-I-W-N-R-D-N-I^{230}
Peptide 3: E^{398}-A-V-Y-T-K-M-M-T-K-K-P-G-M^{411}
Peptide 4: (cyclic); G-K^{407}-K-P-G-M-F-F^{413}-G
Peptide 5: F^{413}-N-P-E-E-S-E-L-D-L-T-Y^{424}
Peptide 6: L^{422}-T-Y-G-N-R-Y-K-N-V^{431}

Peptides 1 and 2 were designed to cover the alpha domain of G6PDH, whereas the remaining ones were designed to cover the beta domain. The beta turn of this domain was utilized to design a cyclic peptide (peptide 4) by adding two glycine residues to the natural sequence of seven residues, thus obtaining a more constrained peptide. The starting structures of the peptide-G6PDH complexes are shown in Fig. 5a–f. Additionally, the structure of the cyclic peptide (peptide 4) is shown in Fig. 6.

To assess the recognition properties of each peptide to G6PDH, molecular dynamics simulations were carried out and the

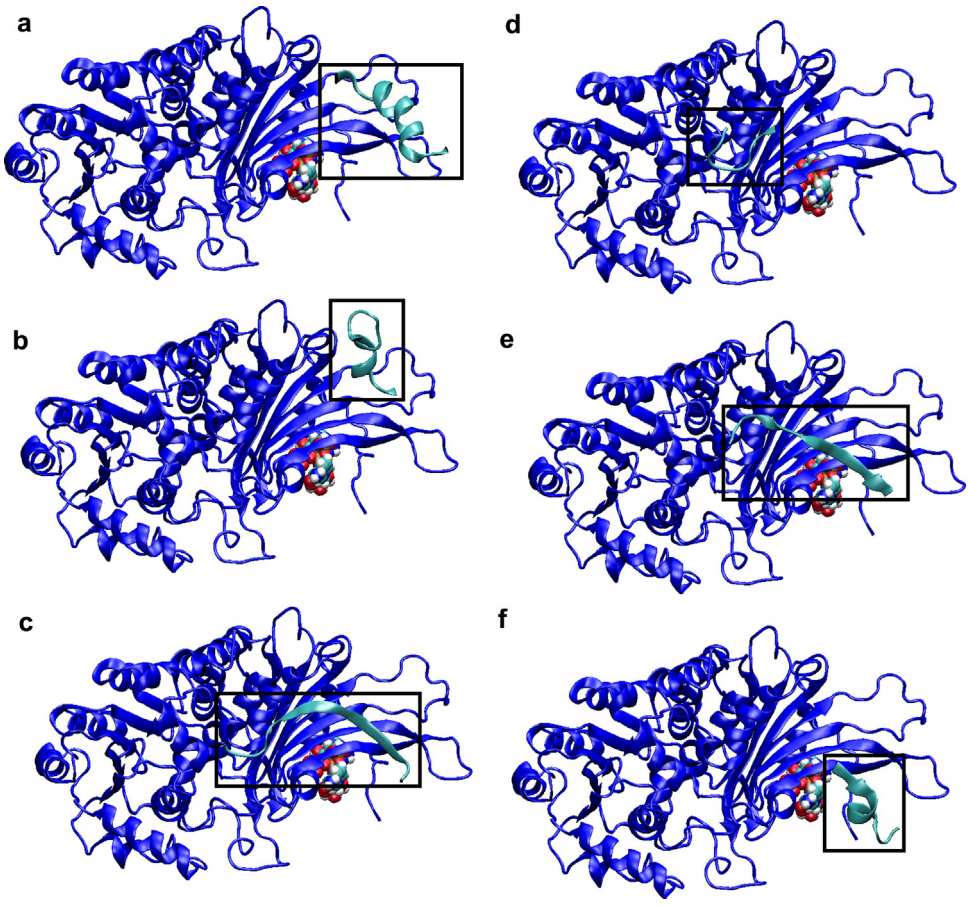

Fig. 5. Starting structures of each peptide-G6PDH complex: peptide 1(a), peptide 2(b), peptide 3(c), peptide 4 before cycled (d), peptide 5(e) and peptide 6(f). For reference of the complete homodimer, see Fig. 1.

production time was used to predict their binding free energies by using the MMPB(GB)SA protocol, as described in Section 2. Results of this analysis are shown in Table 3. Final binding free energies using the PB framework have positive values and thus, the lower they are the better is the affinity of the peptide. This performance was previously obtained in other peptide–protein systems [33] and was mainly argued to be a consequence of the use of Parse radii in its calculation. This set of radii is associated to high desolvation

Table 3
Binding free energy analysis by means of MMPB(GB)SA for the peptide-G6PDH complexes.

kcal/mol	Peptide 1	Peptide 2	Peptide 3	Peptide 4	Peptide 5	Peptide 6
ΔELE	−174.77	−539.84	−164.74	−183.38	−20.08	−406.52
ΔVDW	−60.62	−56.79	−64.98	−40.59	−51.49	−43.79
ΔGAS	−235.39	−596.61	−229.72	−223.98	−71.57	−450.31
ΔPB_{SUR}	−7.26	−7.47	−8.50	−5.39	−6.64	−6.49
ΔPB_{CAL}	235.43	591.61	212.74	215.88	84.14	456.23
ΔPB_{SOL}	228.17	583.87	204.24	210.49	77.50	449.74
ΔPB_{ELE}	60.66	51.50	47.99	32.50	64.06	49.71
ΔPB_{TOT}	−7.22	−12.74	−25.48	−13.49	5.93	−0.57
ΔGB_{SUR}	−8.42	−8.70	−10.07	−5.94	−7.60	−7.40
ΔGB_{CAL}	186.93	528.28	173.27	182.28	36.68	406.90
ΔGB_{SOL}	178.51	519.58	163.21	176.34	29.08	399.50
ΔGB_{ELE}	12.16	−11.55	8.53	−1.10	16.60	0.38
ΔGB_{TOT}	−56.88	−77.03	−66.52	−47.64	−42.49	−50.82
$-T\Delta S_{TRA}$	14.34	14.21	14.27	13.81	14.14	13.96
$-T\Delta S_{ROT}$	13.17	12.81	13.47	12.13	13.29	12.39
$-T\Delta S_{VIB}$	−0.31	1.33	15.50	−1.16	12.39	1.33
$-T\Delta S_{TOT}$	27.20	28.35	43.24	24.78	39.82	27.68
ΔG_{MMPBSA}	19.98	15.61	17.76	11.29	45.75	27.11
ΔG_{MMGBSA}	−29.68	−48.68	−23.28	−22.86	−2.67	−23.14

ΔELE and ΔVDW account for the electrostatic and van der Waals energies extracted from the force field, ΔGAS denotes for ΔELE + ΔVDW, ΔPB_{SUR} is the non polar contribution to solvation using the PB framework, ΔPB_{CAL} is the polar contribution to solvation using the PB framework, ΔPB_{SOL} denotes for $\Delta PB_{SUR} + \Delta PB_{CAL}$ being the total solvation balance, ΔPB_{ELE} accounts for the $\Delta PB_{CAL} + \Delta$ELE which is the total electrostatic final balance, ΔPB_{TOT} accounts for the total enthalpic contribution to binding (ΔGAS + $\Delta PB_{SUR} + \Delta PB_{CAL}$). Same information is provided by the Generalized Born protocol and denoted as GB in the Table. $-T\Delta S_{TRA}$ is the translational entropy, $-T\Delta S_{ROT}$ is the rotational entropy, $-T\Delta S_{VIB}$ is the vibrational entropy and $-T\Delta S_{TOT}$ is the total entropic balance. Finally, ΔG_{MMPBSA} and ΔG_{MMGBSA} denote for the total binding free energy by using the PB and GB frameworks, respectively, calculated at 300 K.

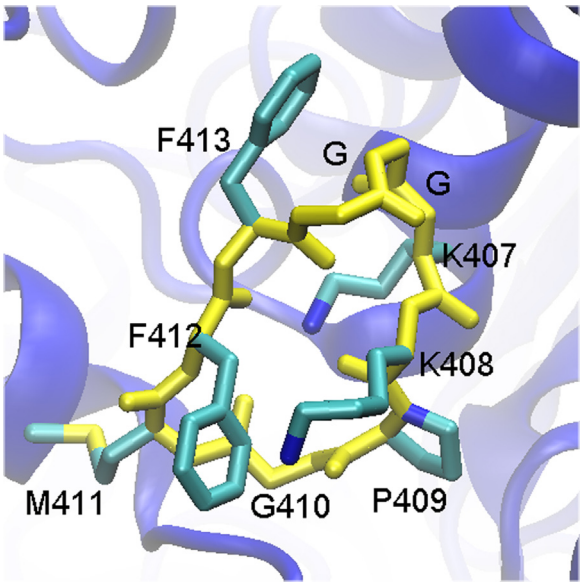

Fig. 6. Detailed view of the cyclic peptide (peptide 4) in complex with G6PDH (backbone shown in yellow and hydrogen atoms not shown for simplicity). (For interpretation of the references to colour in this figure legend, the reader is referred to the web version of this article.)

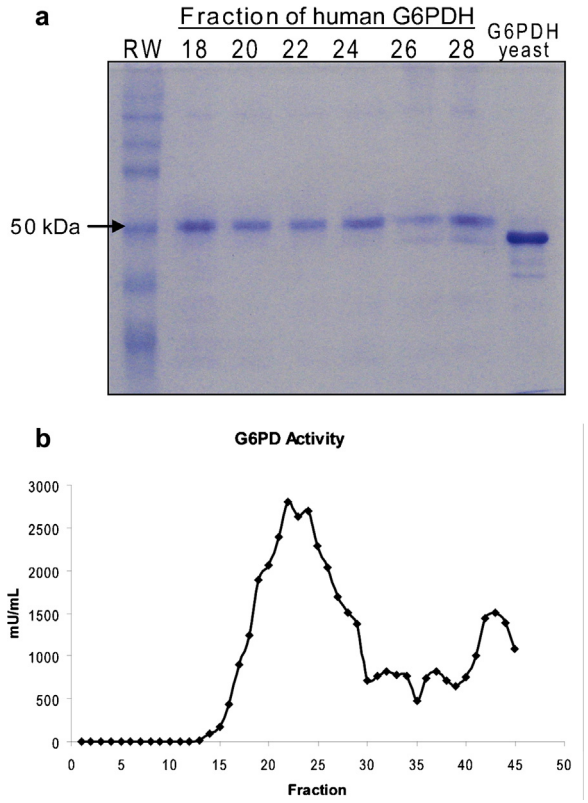

Fig. 7. (a) SDS-PAGE of different fractions of purified human G6PDH. (b) G6PDH activity of the different fractions after purification expressed in mU/mL. The fractions with more activity (18 to 26) were used for *in vitro* experiments.

energies (PB_{CAL}), penalizing in extreme the binding free energy. On the contrary, final binding free energies are negative and probably overestimated within the GB context, although this effect was also previously noticed [34–37]. Due to intrinsic limitation of both methods, only the relative values of binding free energy have to be considered in order to select the peptide candidates for synthesis.

The most active peptides according to the MMPBSA protocol were peptide 3, peptide 4 and peptide 2 (underlined values of Table 3). On its turn, the MMGBSA protocol predicted peptide 1, peptide 2 and peptide 3 as the most promising ones (underlined values of Table 3).

Entropic calculations were almost constant (around 21–28 kcal/mol) for all systems except for peptides 3 and 5, whose entropic penalty decreased the final binding by 43.24 and 39.82 kcal/mol, respectively. Peptide 5 was the less active binder as predicted by both methods and was early discarded.

All in all, we selected peptide 2, peptide 3 and peptide 4 (cyclic) as candidates for synthesis and experimental assays, based on our previous experience [33] that favored the evaluation of PB_{TOT} as the best contribution to correlate predicted with experimental activity in peptide–protein systems (bold values in Table 3). In summary, although entropic effects were calculated, we based our final selection only on the PB_{TOT} contribution, that was optimal for peptides 2, 3 and 4. In fact, entropic terms show generally high deviations among snapshots of the simulation [33] and require extensive computational times making difficult they interpretation. We must insist that the MMPB(GB)SA protocol can only be used as an aid to the final selection of peptide candidates and that interactions of these peptides with the protein have to be taken into account too. Thus, peptides 2, 3 and 4 were also favored by extensive interactions with the G6PDH monomer.

5. Experimental assay

5.1. G6PDH activity determination and inhibition assay

Human G6PDH was obtained, purified and evaluated as described in Section 2. Results showed a good G6PDH purification as it is demonstrated by a unique band in the gel of the selected fractions eluting from the affinity chromatography column (Fig. 7a). The evaluation of the activity of purified G6PDH showed that the most active fractions were from 18 to 26 (Fig. 7b). These fractions were used for the inhibition assays.

The three compounds described (peptides 2, 3 and 4) were synthesized and tested by spectrophotometric methods for G6PDH activity inhibition (see Section 2). Peptide 2 exhibited a low activity with an IC_{50} (peptide concentration that inhibits 50% of the enzyme activity) over 250 μM. Similarly, peptide 4 only inhibited 5% of G6PDH activity at 250 μM. On the contrary, peptide 3 showed a remarkable inhibition of human G6PDH. The IC_{50} of peptide 3 was estimated in 50 μM. Moreover, a peptide concentration of 60 μM inhibited the enzymatic activity by 83% (IC_{80} estimated in 60 μM). Peptide 3, designed and tested in this study, represents a novel compound for developing human G6PDH inhibitors.

5.2. Detailed binding mode of peptide 3 in complex with G6PDH

The binding mode of the active peptide 3 was deeper analyzed by molecular modeling (Fig. 8) in order to provide interaction points useful for future design of peptidomimetic molecules and to perform structure-based virtual screening. Additionally, the natural sequence of the peptide can be modified by designing point mutations improving the interaction features, reducing flexibility and enhancing therefore the binding affinity. Peptide 3 maintained nine stable hydrogen bonds throughout the molecular dynamics simulation, distributed among residues M405 (two hydrogen bonds with N218), T406 (two hydrogen bonds with N210 and Y424), K407 (four hydrogen bonds with E296, N210 and Y424) and G410 (a single hydrogen bond with E206). Table 4 summarizes the geometric parameters of these nine hydrogen bonds during molecular dynamics. Electrostatic recognition was practically guided by residue K407

Table 4
List of hydrogen bonds formed between peptide 3 and the G6PDH monomer.

Peptide 3	G6PDH monomer	% Occupancy	Average distance/Å	Distance RMS/Å	Average angle/°	Angle RMS/°
T406 O sc	N210 NH sc	45.6	2.11	0.21	148.3	12.5
M405 O mc	N218 NH sc	80.8	2.86	0.16	158.5	10.2
K407 O mc	Y424 OH sc	88.8	1.77	0.13	160.9	10.1
M405 NH mc	N218 O sc	74.0	1.96	0.16	156.4	11.7
T406 OH sc	Y424 OH sc	79.2	1.93	0.17	157.5	12.0
K407 NH sc	E206 O sc	39.4	2.62	0.82	102.8	53.3
K407 NH sc	E296 O sc	31.2	2.72	0.71	95.4	51.5
K407 NH mc	N210 sc	81.2	1.94	0.14	157.2	10.1
G410 NH mc	E206 sc	51.8	2.44	0.68	156.3	12.5

Per cent of occupancy defines the total simulation time that the geometry of the hydrogen bond is optimum: N-O distance < 3.3 Å and hydrogen bond angle between 180 ± 20°. Average distance denotes for hydrogen-heavy atom distance, distance RMS is the distance deviation, average angle is the heavy atom-hydrogen-heavy atom angle and angle RMS denotes the angle deviation, all parameters calculated from molecular dynamics. In this table, "sc" denotes for a side chain atom, whereas "mc" denotes for a main chain atom.

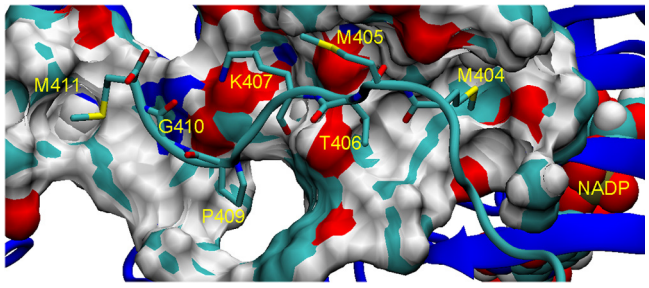

Fig. 8. Detailed binding mode of peptide 3 in complex with G6PDH, showing the residues which provided the main interactions (hydrogen atoms not shown for simplicity).

that provided around −35 kcal/mol, whereas van der Waals contacts were extensively distributed along the entire peptide, being M404, P409 and M411 the most remarkable residues, providing around −7, −9 and −10 kcal/mol, respectively. Moreover, peptide 3 could inhibit G6PDH by means of an allosteric mechanism since the binding site of this peptide is close to the catalytical site of the enzyme containing the $NADP^+$, making feasible its distortion [13,15].

6. Conclusions

By using a computational protocol based on i) analyzing the protein–protein interface by molecular dynamics, ii) designing interface peptides retaining the strongest interactions, iii) predicting their binding free energies and iv) assaying experimentally the most promising candidates, we have discovered a new peptide interface inhibitor of human G6PDH, a novel target for cancer drug development involved into the pentose phosphate pathway. The linear active peptide of 14 residues derived from the beta domain (peptide 3) inhibited the protein with an IC_{50} of 50 μM and IC_{80} of 60 μM. Although its activity is only modest, the designed peptide and its proposed binding site and binding mode can be used for the future rational design of peptidomimetics that could lead to new potent human G6PDH inhibitors since the designed peptide highlights a new strategy for inhibiting the enzyme.

Acknowledgments

The authors thank Ms. Ursula Valls for technical assistance in the experiments. This work was supported by the Spanish government, Spanish Ministry of Science and Innovation & European Regional Development Fund (projects CTQ2011-29285-C02-02 and SAF2011-25726) and the AGAUR-Generalitat de Catalunya (project 2009SGR1308 and Icrea Academia Award 2010 granted to M.C.). Human G6PDH plasmid was a generous gift of Dr. Bautista.

References

[1] E. Paul, M.D. Carson, M.D. Frischer, Glucose-6-phosphate dehydrogenase deficiency and related disorders of the pentose phosphate pathway, American Journal of Medicine 41 (1966) 744–761.
[2] J. Boren, A. Ramos-Montoya, P. De Atauri, B. Comin-Anduix, A. Cortes, J.J. Centelles, W.M. Fredericks, C.J.F. Van Noorden, M. Cascante, Metabolic control analysis aimed at the ribose synthesis pathway of tumor cells: a new strategy for antitumor drug development, Molecular Biology Reports 29 (2002) 7–12.
[3] M.L. Cheng, H.Y. Ho, Y.H. Wu, D.T. Chiu, Glucose-6-phosphate dehydrogenase-deficient cells show an increased propensity for oxidant-induced senescence, Free Radical Biology and Medicine 36 (2004) 580–591.
[4] L.P. Gao, M.L. Cheng, H.J. Chou, Y.H. Yang, H.Y. Ho, D.T. Chiu, Ineffective GSH regeneration enhances G6PD-knockdown Hep G2 cell sensitivity to diamide-induced oxidative damage, Free Radical Biology & Medicine 47 (2009) 529–535.
[5] H.Y. Ho, M.L. Cheng, D.T. Chiu, Glucose-6-phosphate dehydrogenase-from oxidative stress to cellular functions and degenerative diseases, Redox Report 12 (2007) 109–118.
[6] B.L. Horecker, The pentose phosphate pathway, The Journal of Biological Chemistry 277 (2002) 47965–47971.
[7] W.M. Frederiks, P. Vizan, K.S. Bosch, H. Vreeling-Sindelarova, J. Boren, M. Cascante, Elevated activity of the oxidative and non-oxidative pentose phosphate pathway in (pre)neoplastic lesions in rat liver, International Journal of Experimental Pathology 89 (2008) 232–240.
[8] R.M. Babiak, A.P. Campello, E.G. Carnieri, M.B. Oliveira, Methotrexate: pentose cycle and oxidative stress, Cell Biochemistry and Function 4 (1998) 283–293.
[9] A. Ramos-Montoya, W.N. Lee, S. Bassilian, S. Lim, R.V. Trebukhina, M.V. Kazhyna, C.J. Ciudad, V. Noe, J.J. Centelles, M. Cascante, Pentose phosphate cycle oxidative and nonoxidative balance: a new vulnerable target for overcoming drug resistance in cancer, International Journal of Cancer 119 (2006) 2733–3274.
[10] C. Asensio, N. Levoin, C. Guillaume, M.J. Guerquin, K. Rouguieg, F. Chretien, Y. Chapleur, P. Netter, A. Minn, F. Lapicque, Irreversible inhibition of glucose-6-phosphate deshydrogenase by the coenzyme A conjugate of ketoprofen: a key to oxidative stress induced by non-steroidal anti-inflammatory drugs? Biochemical Pharmacology 73 (2007) 405–416.
[11] M. Cifti, M.E. Buyukokuroglu, O.I. Kufrevioglu, Effect of cefaperazone/sulbactam and ampicillin/sulbactam on the *in vitro* activity of human erythrocyte glucose-6-phosphate dehydrogenase, Journal of Basic and Clinical Physiology and Pharmacology 12 (2001) 305–313.
[12] M. Cifti, I. Ozmen, M.E. Buyukokuroglu, S. Pence, O.I. Kufrevioglu, Effects of metamizol and magnesium sulfate on enzyme activity of glucose-6-phosphate dehydrogenase from human erythrocyte *in vitro* and rat erythrocyte *in vivo*, Clinical Biochemistry 34 (2001) 297–302.
[13] S.W. Au, S. Gover, V.M. Lam, M.J. Adams, Human glucose-6-phosphate dehydrogenase: the crystal structure reveals a structural NADP(+) molecule and provides insights into enzyme deficiency, Structure 8 (2000) 293–303.
[14] D. Cardinale, O.M. Salo-Ahen, S. Ferrari, G. Ponterini, G. Cruciani, E. Carosati, A.M. Tochowicz, S. Mangani, R.C. Wade, M.P. Costi, Homodimeric enzymes as drug targets, Current Medicinal Chemistry 17 (2010) 826–846.
[15] D.A. Scopes, J.M. Bautista, C.E. Naylor, M.J. Adams, P.J. Mason, Amino acid substitution at the dimer interface of human glucose-6-phosphate dehydrogenase that increase thermostability and reduce the stabilising effect of NADP, European Journal of Biochemistry 251 (1998) 382–388.
[16] J.A. Wells, C.L. McClendon, Reaching for high-hanging fruit in drug discovery at protein-protein interfaces, Nature 450 (2007) 1001–1009.
[17] H. Nakajima, N. Mizuta, K. Sakaguchi, I. Fujiwara, A. Yoshimori, S. Takahasi, R. Takawasa, S. Tanuma, Development of HER2-antagonistic peptides as novel anti-breast cancer drugs by *in silico* methods, Breast Cancer 15 (2008) 65–72.
[18] V. Prasanna, S. Bhattacharjya, P. Balaram, Synthetic interface peptides as inactivators of multimeric enzymes: inhibitory and conformational properties of three fragments from *Lactobacillus casei* thymidylate synthase, Biochemistry 37 (1998) 6883–6893.
[19] W. Cui, Z. Wei, Q. Chen, Y. Cheng, L. Geng, J. Zhang, J. Chen, T. Hou, M. Ji, Structure-based design of peptides against G3BP with cytotoxicity on tumor cells, Journal of Chemical Information and Modeling 50 (2010) 380–387.

[20] S. Gordo, E. Giralt, Knitting and untying the protein network: modulation of protein ensembles as a therapeutic strategy, Protein Science 18 (2009) 481–493.
[21] W.D. Cornell, P. Cieplak, C.L. Bayly, I.R. Goud, K.M. Mertz Jr., D.M. Ferguson, D.C. Spellmeyer, T. Fox, J.W. Caldwell, P.A. Kollman, A second generation force field for the simulation of proteins, nucleic acids, and organic molecules, Journal of the American Chemical Society 117 (1995) 5179–5197.
[22] D.A. Case, T.A. Darden, T.E. Cheatham III, C.L. Simmerling, J. Wang, R.E. Duke, R. Luo, M. Crowley, R.C. Walker, W. Zhang, K.M. Merz, B. Wang, S. Hayik, A. Roitberg, G. Seabra, I. Kolossváry, K.F. Wong, F. Paesani, J. Vanicek, X. Wu, S.R. Brozell, T. Steinbrecher, H. Gohlke, L. Yang, C. Tan, J. Mongan, V. Hornak, G. Cui, D.H. Mathews, M.G. Seetin, C. Sagui, V. Babin, P.A. Kollman, AMBER 10, University of California, San Francisco, 2008.
[23] T. Darden, D. York, L. Pedersen, Particle mesh Ewald: an N log (N) method for Ewald sums in large systems, The Journal of Chemical Physics 98 (1993) 10089–10092.
[24] W. Humphrey, A. Dalke, K. Schulten, VMD - Visual molecular dynamics, Journal of Molecular Graphics and Modelling 14 (1996) 33–38.
[25] N. Holmberg, U. Ryde, L. Bulow, Redesign of the coenzyme specificity in L-lactate dehydrogenase from *Bacillus sarothermophilus* using site-directed mutagenesis and media engineering, Protein Engineering Design and Selection 12 (1999) 851–856.
[26] H.J.C. Berendsen, J.P.M. Postman, W.F. Van Gunsteren, A. DiNola, J.R. Haak, Molecular dynamics with coupling to an external bath, The Journal of Chemical Physics 81 (1984) 3684–3690.
[27] J.P. Ryckaert, G. Ciccotti, H.J. Berendsen, Numerical integration of the Cartesian equations of motion of a system with constraints: molecular dynamics of n-alkanes, Journal of Computational Chemistry 23 (1977) 327–341.
[28] P.A. Kollman, I. Massova, C. Reyes, B. Kuhn, S. Huo, L. Chong, M. Lee, T. Lee, Y. Duan, W. Wang, O. Donini, J. Srivasan, D.A. Case, T.E. Cheatam III, Calculating structures and free energies of complex molecules: combining molecular mechanics and continuum models, Accounts of Chemical Research 33 (2000) 889–897.
[29] V. Tsui, D.A. Case, Theory and applications of the generalized Born solvation model in macromolecular simulations, Biopolymers 56 (2001) 275–291.
[30] J.M. Bautista, P.J. Mason, L. Luzzatto, Purification and properties of human glucose-6-phosphate dehydrogenase made in *E. coli*, Biochimica et Biophysica Acta 1119 (1992) 74–80.
[31] M. Town, J.M. Bautista, P.J. Mason, L. Luzzatto, Both mutations in G6PD A- are necessary to produce the G6PD deficient phenotype, Human Molecular Genetics 1 (1992) 171–174.
[32] W.N. Tian, L.D. Braunstein, J. Pang, K.M. Stuhlmeier, Q.C. Xi, X. Tian, R.C. Stanton, Importance of glucose-6-phosphate dehydrogenase activity for cell growth, The Journal of Biological Chemistry 273 (1998) 10609–10617.
[33] C. Obiol-Pardo, J. Rubio-Martinez, Comparative evaluation of MMPBSA and XSCORE to compute binding free energy in XIAP-peptide complexes, Journal of Chemical Information and Modeling 47 (2007) 134–142.
[34] C. Obiol-Pardo, J.M. Granadino-Roldan, J. Rubio-Martinez, Protein-protein recognition as a first step towards the inhibition of XIAP and Survivin anti-apoptotic proteins, Journal of Molecular Recognition 21 (2008) 190–204.
[35] C. Obiol-Pardo, J. Rubio-Martinez, Homology modeling of human transketolase: description of critical sites useful for drug design and study of the cofactor binding mode, Journal of Molecular Graphics and Modelling 27 (2009) 723–734.
[36] C. Obiol-Pardo, A. Cordero, J. Rubio-Martinez, S. Imperial, Homology modeling of *Mycobacterium tuberculosis* 2C-methyl-D-eryhthritol-4-phosphate cytidylyltransferase, the third enzyme in the MEP pathway for isoprenoid biosynthesis, Journal of Molecular Modeling 16 (2010) 1061–1073.
[37] V. Gimenez-Oya, O. Villacañas, C. Obiol-Pardo, M. Antolin-Llovera, J. Rubio-Martinez, S. Imperial, Design of novel ligands of CDP-methylerythritol kinase by mimicking direct protein-protein and solvent-mediated interactions, Journal of Molecular Recognition 24 (2011) 71–80.